



Geophysical Research Letters°



RESEARCH LETTER

10.1029/2022GL098031

Key Points:

- We show for the first time that there is an explicit By-dependence in the ring current/proton precipitation and in the inner magnetosphere
- During Northern Hemisphere summer (winter) the ring current fluxes/proton precipitation and the rate of change of the *Dst* index are stronger for B_y < 0 (B_y > 0)
- The B_y-dependence of the ring current and energetic proton fluxes is reproduced by a global coupled MHD-ring current model

Supporting Information:

Supporting Information may be found in the online version of this article.

Correspondence to:

L. Holappa, lauri.holappa@oulu.fi

Citation:

Holappa, L., & Buzulukova, N. Y. (2022). Explicit IMF B_y -dependence of energetic protons and the ring current. *Geophysical Research Letters*, 49, e2022GL098031. https://doi.org/10.1029/2022GL098031

Received 24 JAN 2022 Accepted 15 APR 2022

© 2022 The Authors.

This is an open access article under the terms of the Creative Commons Attribution-NonCommercial License, which permits use, distribution and reproduction in any medium, provided the original work is properly cited and is not used for commercial purposes.

Explicit IMF B_y -Dependence of Energetic Protons and the Ring Current

L. Holappa^{1,2,3} and N. Y. Buzulukova^{2,3}

¹Space Physics and Astronomy Research Unit, University of Oulu, Oulu, Finland, ²University of Maryland, College Park, MD, USA, ³NASA Goddard Space Flight Center, Greenbelt, MD, USA

Abstract The most important parameter driving the solar wind-magnetosphere interaction is the southward (B_z) component of the interplanetary magnetic field (IMF). While the dawn-dusk (B_y) component of the IMF is also known to play an important role, its effects are usually assumed to be independent of its sign. Here we demonstrate for the first time a seasonally varying, explicit IMF B_y -dependence of the ring current and Dst index. Using satellite observations and a global magnetohydrodynamic model coupled with a ring current model, we show that for a fixed level of solar wind driving the flux of energetic magnetospheric protons and the growth-rate of the ring current are greater for $B_y < 0$ ($B_y > 0$) than for $B_y > 0$ ($B_y < 0$) in Northern Hemisphere summer (winter). While the physical mechanism of this explicit B_y -effect is not yet fully understood, our results suggest that IMF B_y modulates magnetospheric convection and plasma transport in the inner magnetosphere.

Plain Language Summary The magnetic field carried by solar wind is the most important driver of space weather. Aurora and other phenomena in the near-Earth space are known to be stronger when the magnetic field on solar wind points to south than north. Usually the space weather response is expected to be equally strong for eastward and westward magnetic fields in solar wind. In this paper show that this is not the case. Using satellite measurements and computer modeling we show that electric currents in the near-Earth space are stronger for westward than eastward magnetic field in solar wind in northern hemisphere summer, while the opposite is true in northern hemisphere winter. More studies are needed for understanding the physical mechanism of this phenomenon.

1. Introduction

The interaction between solar wind, interplanetary magnetic field (IMF) and the Earth's magnetic field is dominated by the north-south (B_z) component of IMF, which is the most important driver of dayside reconnection (Dungey, 1961), and thus the energy input into the magnetosphere. The dawn-dusk (B_o) component of IMF is also known play an important role, leading, for example, to a B_y -dependence of the ionospheric convection patterns (Cowley et al., 1991; Heppner & Maynard, 1987; Ruohoniemi & Greenwald, 2005; Thomas & Shepherd, 2018). It is also known that IMF B_v modulates the dayside reconnection rate by affecting, for example, the geometry of the merging line (Laitinen et al., 2007; Sonnerup, 1974; Trattner et al., 2012), its effect on the magnetospheric response is usually assumed to be symmetric with respect to its sign. For example, all empirical solar wind coupling functions assume a symmetric dependence on IMF B_v (Kan & Lee, 1979; Newell et al., 2007; Perreault & Akasofu, 1978). However, several magnetospheric and ionospheric phenomena are known to respond differently to positive and negative IMF B_v . For example, a negative IMF B_v component results in larger nightside auroral intensity in the Northern Hemisphere (NH; Liou et al., 1998; Shue et al., 2001) while the effect is reversed in the southern hemisphere (Liou & Mitchell, 2019). On dayside, the postnoon auroral bright spot is brighter for negative IMF B_y than for positive IMF B_y and the effect is reversed in the southern hemisphere (Liou & Mitchell, 2019) Also several studies (Friis-Christensen et al., 1972, 2017; Holappa & Mursula, 2018; Murayama et al., 1980; Smith et al., 2017; Workayehu et al., 2021; Holappa et al., 2021) have shown that there is a strong IMF B_v -dependence in auroral currents which is not symmetric with the B_v sign. This so-called explicit B_v -dependence is especially strong in the AL index (measuring the westward electrojet), which is about 40% stronger for $B_y > 0$ than for $B_y < 0$ in NH winter, or under negative tilt angle of the Earth's magnetic dipole with respect to the Sun-Earth line. Similar B_y -dependence has also been found in the substorm onset frequency and intensity (Liou et al., 2020; Ohma et al., 2021; Velichko et al., 2002). In NH summer (or during positive dipole tilt) the B,-dependence is reversed.



The B_y -dependence of the auroral electrojets is at least partly due to a B_y -dependence of electron precipitation and ionospheric conductance. Holappa et al. (2020) showed that the fluxes of energetic (>30 keV) precipitating electrons in the dawn sector (measured by the National Oceanic and Atmospheric Administration (NOAA) Polar Operational Environmental satellites, POES) are modulated by IMF B_y similarly as the westward electrojet (greater precipitation for $B_y < 0$ in NH summer and $B_y > 0$ in NH winter). The B_y -dependence of electron precipitation implies a similar B_y -dependence of ionospheric conductance. Recent studies (Holappa et al., 2021; Weimer & Edwards, 2021) have indeed found a similar IMF B_y -dependence of ionospheric conductance, maximizing in the dawn sector.

The physical mechanism of the explicit B_y -effect is still not fully understood. As the above recent studies indicate, understanding how IMF B_y modulates the magnetospheric energetic particles and their precipitation into ionosphere are of key importance. An important question is whether the ring current also exhibits an explicit B_y -dependence. Possible explicit IMF B_y effects in the inner magnetosphere have not been analyzed, although it has been suggested that IMF B_y plays a role in skewing of the inner magnetosphere electric field as observed in Energetic Neutral Atom (ENA) emissions (C:son Brandt et al., 2002).

A viable method for studying the coupling between IMF B_y and the ring current is to use first-principles numerical models, such as global magnetohydrodynamic (MHD) models coupled with the ring current models of the inner magnetosphere (Buzulukova, Fok, Pulkkinen, et al., 2010; de Zeeuw et al., 2004; Glocer et al., 2013; Tóth et al., 2005; Zhang et al., 2007). While the MHD physics is not sufficient for describing energetic particle populations, the global MHD models can be coupled with kinetic inner magnetosphere models, such as the Comprehensive Inner Magnetosphere-Ionosphere (CIMI) model (M. C. Fok et al., 2014, 2021), designed for modeling the ring current and radiation belt physics.

The goal of this paper is to quantify the B_y -dependence of magnetospheric electrons and protons and the ring current using global modeling with a coupled model and satellite measurements. We will use the Space Weather Modeling Framework (SWMF) (Tóth et al., 2005) coupled with the CIMI model. With this capability we are able to model also the B_y -dependence of the ring current fluxes. We will compare the modeling results to NOAA POES measurements of energetic magnetospheric protons and the Dst index.

This paper is organized as follows. In Section 2 we will introduce the data and the models in our analysis. The results from the global coupled model and satellite measurements are given in Sections 3 and 4, respectively. Finally we discuss our results and give our conclusions in Section 5.

2. Data and Methods

2.1. Global 3D MHD BATS-R-US Model Coupled With CIMI

We use the global 3D BATS-R-US MHD code (Powell et al., 1999; Tóth et al., 2012) coupled with the CIMI model (M. C. Fok et al., 2014) and Ridley ionospheric electrodynamics (RIM) module (Ridley et al., 2004). BATS-R-US, CIMI and RIM are parts of SWMF developed at University of Michigan (Tóth et al., 2005). For this study we use an ideal one-fluid anisotropic version of BATS-R-US MHD with grid resolution $1/8~R_E$ in the near-Earth region inside $r < 13~R_E$. The total number of grid points is $\sim 8 \times 10^6$. It is acknowledged that magnetic field reconnection in ideal MHD model is defined by numerical resistivity, however multiple studies of substorms with different MHD codes (Birn & Hesse, 2013; Fedder et al., 1995; Gordeev et al., 2017; Keesee et al., 2021; Merkin et al., 2019; Raeder et al., 2010) confirm that this approach works reasonably well for the Earth's magnetosphere (although with some caveats). Global MHD model provides a reasonable solution for 3D structure of currents, magnetic field and plasma parameters (bulk velocity, pressure and density). In the inner magnetosphere, additional physics should be included to describe the ring current effects. This is done by dynamic two-way coupling of MHD solution and the ring current solution in order to describe energy-dependent gradient drifts of the ring current population with energies $\sim 1-200~\text{keV}$. Details of the coupling methodology can be found in (de Zeeuw et al., 2004; Glocer et al., 2013).

Solution for ionospheric electric field potential is provided by RIM with ionospheric conductivity calculated from an empirical relation between field-aligned currents and ionospheric conductivity specified with the Assimilative Mapping of Ionospheric Electrodynamics model (Ridley et al., 2004).

HOLAPPA AND BUZULUKOVA 2 of 11



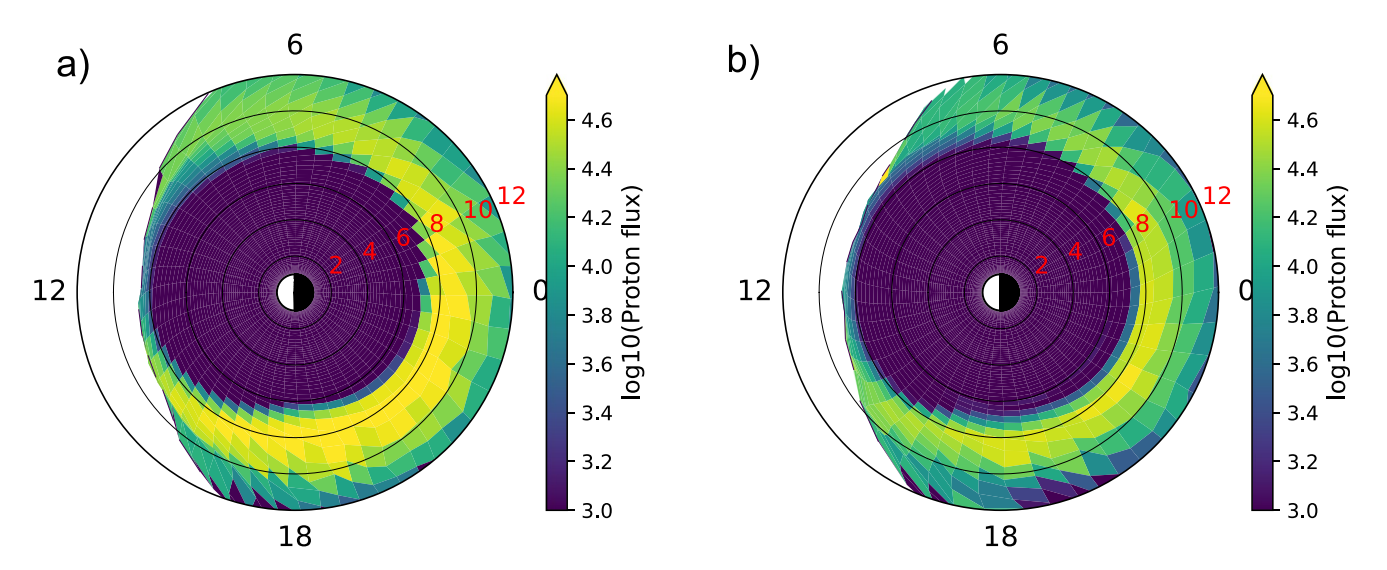


Figure 1. Equatorial omnidirectional fluxes of 56 keV protons for (a) the run with $B_y < 0$ (b) $B_y > 0$. Flux units are $1/\text{cm}^2/\text{sr/s/keV}$ in log-10 scale. The fluxes are shown for the last timesteps (8.00 hr) of the two runs. Sun is from the left. Labels indicate magnetic local time and radial distance (in Earth radii).

In this paper we present the results of two runs with positive/negative IMF Geocentric Solar Magnetospheric (GSM) $B_y = +5/-5$ nT for the dipole tilt 20° in XZ GSM plane, corresponding to summer in NH. The value of tilt is kept fixed through the two runs. Except IMF B_y all run parameters are identical in the two runs. Two runs are made with static IMF input solar wind $V_x = -500$ km/s; $V_y = V_z = 0$; IMF $B_x = 0$; solar wind density n = 3 cm⁻³; solar wind temperature T = 200,000 K. The first 2 hr of simulations are done with $B_z = 3$ nT, and the next 6 hr of simulations are done with static $B_z = -5$ nT.

2.2. NOAA POES Data and Dst Index Data

In this paper we use energetic particle measurements from NOAA15-NOAA19 satellites in 1995–2019. The measurements from different NOAA satellites have been calibrated for instrument degradation and other issues (Asikainen & Mursula, 2011, 2013). The POES satellites measure protons with two orthogonal (0° and 90°) detectors. While the 0° detector mainly measures precipitating particles in high latitudes, the 90° detector measures a mixture of trapped and precipitating particles, depending on location (Rodger et al., 2010). To compare the POES measurements to the modeled omnidirectional proton fluxes we average the 0° and 90° fluxes of the lowest energy channel (30–80 keV). We note that it is not possible to strictly resolve trapped or precipitating fluxes of protons from POES measurements. Therefore we will also study the 0° and 90° telescope measurements separately.

To quantify the intensity of the ring current we use the *Dst* index downloaded from NASA GSFC's OmniWeb server.

3. Results: IMF B_{ν} Effect in CIMI Fluxes and Energy Content

Figures 1a and 1b show the omnidirectional fluxes of 56 keV protons for the last timestep (8.00 hr) of the two runs at the geomagnetic equatorial plane (minimum B field plane) for $B_y = +5$ nT and $B_y = -5$ nT, calculated from CIMI output. For two runs with different By the proton flux is stronger in the premidnight and dusk sectors than in the dawn sector. This reflects the well-known dawn-dusk asymmetry of the ring current during the storm main phase (Buzulukova, Fok, Goldstein, et al., 2010; Hamilton et al., 1988; Liemohn et al., 2001; Yakovchouk et al., 2012).

In addition to well-known dawn-dusk ring current asymmetry, proton fluxes in Figure 1 exhibit a strong B_y -dependence. The proton fluxes are greater for negative B_y than for positive B_y . This B_y -dependence is strongest in the dusk and premidnight sectors where the fluxes are also largest overall. Figure S1 in Supporting Information S1 is similar to Figure 1 shows that the omnidirectional (56 keV) electron flux in the dawn sector exhibits a similar

HOLAPPA AND BUZULUKOVA 3 of 11



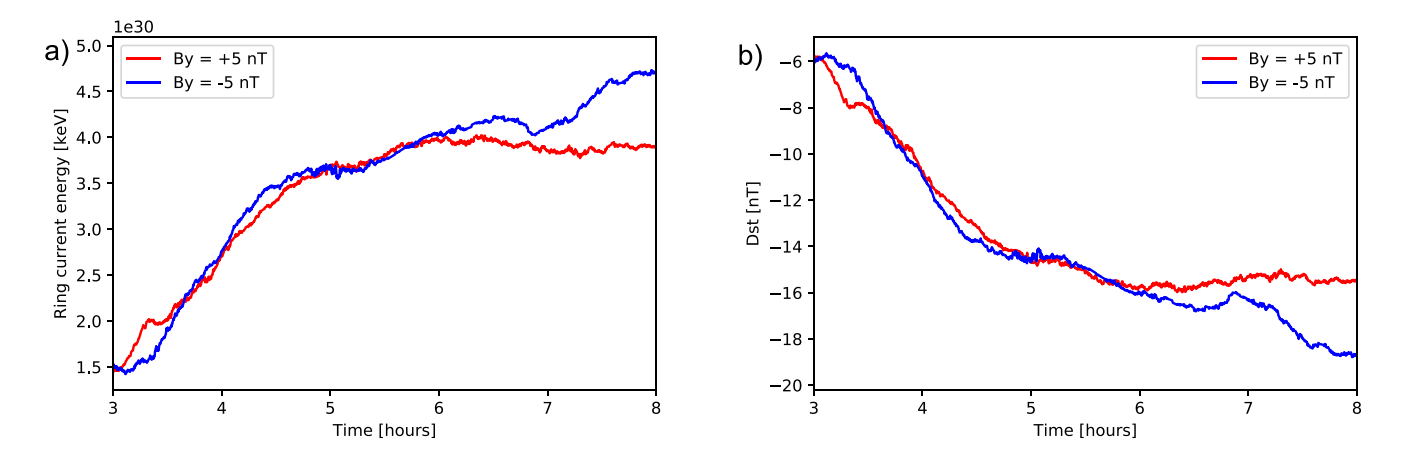


Figure 2. (a) Simulated total energy of the ring current protons as a function of the simulation time for the signs of interplanetary magnetic field B_y . (b) Dst^* indices calculated from the total proton energy using the Dessler-Parker-Sckopke relationship.

 B_y -dependence as protons in the dusk sector, showing larger value of fluxes for the run with negative B_y , in agreement with earlier based on NOAA POES measurements of >30 keV electrons (Holappa et al., 2020).

Figure 2a shows the total energy content of the ring current calculated from the proton CIMI model for the two runs with opposite polarities of IMF B_y after the IMF B_z is turned southward at t=2 hr. While the evolution of ring current energy is very similar for both signs of IMF B_y during t=3..6 hr, negative B_y yields clearly greater ring current energy during the last 2 hr of the runs. The same B_y -dependence is seen in Figure 2b, which shows the pressure-corrected Dst indices (Dst^*) (O'Brien & McPherron, 2000) calculated from the ring current energies (U) in Figure 2a by the Dessler-Parker-Sckopke (DPS) relationship ($Dst^*=3.98 \cdot 10^{-30} \cdot U$ [keV]) (Dessler & Parker, 1959).

Both Figures 1 and 2 demonstrate that the ring current fluxes, energy content and the modeled Dst index show explicit IMF B_y -dependence with stronger ring current and larger fluxes for negative B_y in NH summer. Figure S2 in Supporting Information S1 shows the Dst indices for the two runs computed by Bio-Savart integrals, including contributions of all current systems. Figure S2 in Supporting Information S1 shows a similar B_y -dependence as Figure 1. However, the Dst indices in Figure S2 in Supporting Information S1 are positive during both runs, likely due to a lower dayside reconnection rate in this particular MHD setup, and, therefore, a stronger contribution of the magnetopause current.

4. Results: IMF B_y -Effect in Measured Energetic Protons and the *Dst* Index

To support and extend results presented in the previous section, we study the B_y -dependence of energetic (30–80 keV) protons, measured by NOAA POES satellites. For quantifying the B_y -dependence of the particle fluxes we use similar methodology as Holappa et al. (2020), by sorting the measured particle fluxes by IMF B_y and the Newell et al. (2007) coupling function, designed to represent the dayside reconnection rate at the magnetopause (MP)

$$\frac{d\Phi_{MP}}{dt} = v^{4/3} B_T^{2/3} \sin(\theta/2)^{8/3},\tag{1}$$

where $B_T = \sqrt{B_z^2 + B_y^2}$ and $\theta = \arctan B_y/B_z$ is the IMF clock-angle. This coupling function is dominated by IMF B_z , but it also includes IMF B_y . However, the Newell function (as all other coupling functions) is symmetric with respect to the sign of B_y .

Figures 3a and 3b show the average 30–80 keV proton fluxes (average of the 0° and 90° telescopes) in both hemispheres under positive (>20°) dipole tilt. The proton fluxes are averaged over the dusk sector (12–24 MLT) and $\pm (55^{\circ}...75^{\circ})$ corrected geomagnetic latitude, roughly corresponding to L=3-10, which are the MLT and L-ranges with highest fluxes of protons in the CIMI results in Figure 1. The proton fluxes are binned by the Newell coupling function $d\Phi_{MP}/dt$ and IMF B_{ν} averaged over 3 hr prior the proton measurements.

HOLAPPA AND BUZULUKOVA 4 of 11



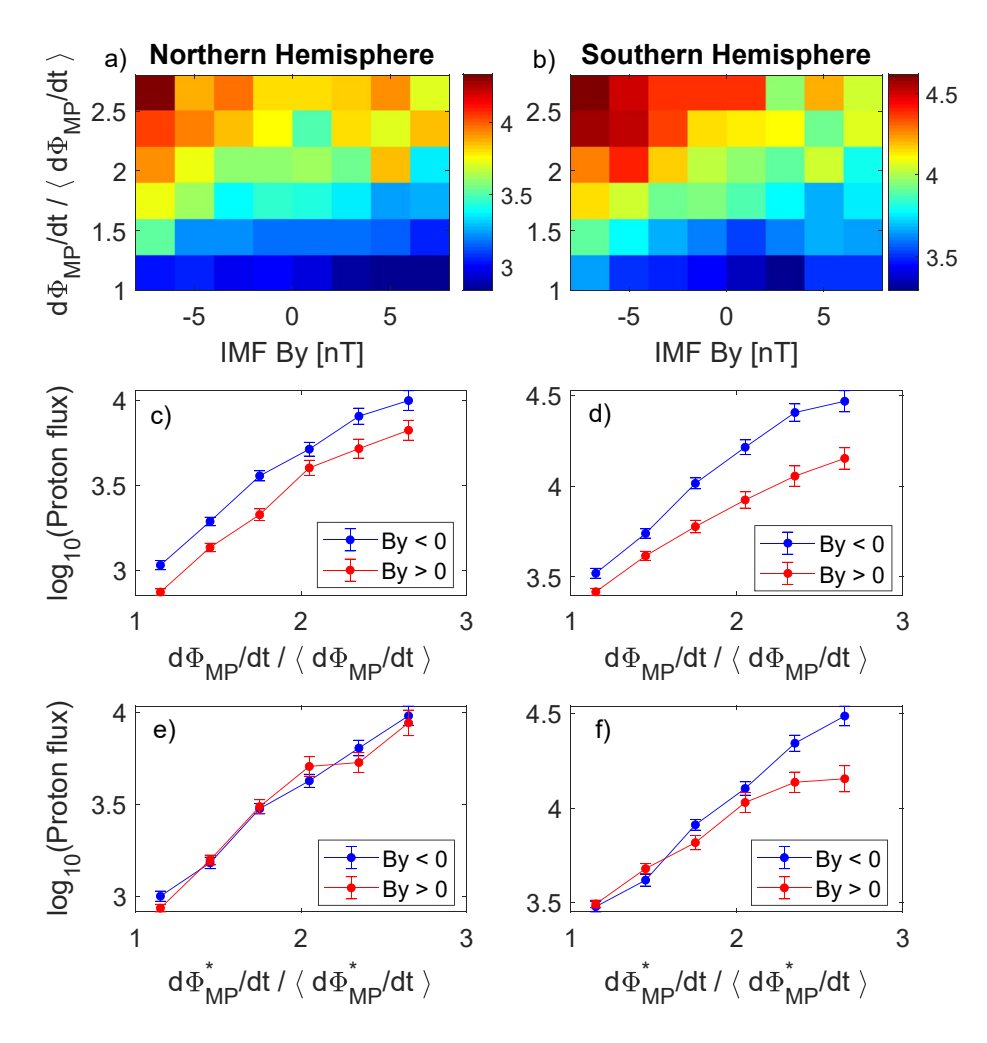


Figure 3. Flux of 30–80 keV protons measured by NOAA POES satellites as a function of the Newell coupling function $d\Phi_{MP}/dt$ and interplanetary magnetic field B_y (averaged over 3 previous hours) during NH summer conditions (dipole tilt >20°) (a) in NH (55°...70° corrected geomagnetic latitude) (b) Southern Hemisphere (-55°...-75° corrected geomagnetic latitude). The units are $1/\text{cm}^2/\text{sr/s}$ in log-10 scale. The Newell coupling function is normalized by its mean value in 1995–2019 $\langle d\Phi_{MP}/dt \rangle = 3.781 \cdot 10^3 \, (\text{km/s})^{4/3} \, \text{nT}^2/3$. (c and d) Proton fluxes (a and b) in averaged for $B_y < 0$ and $B_y > 0$ as a function of $d\Phi_{MP}/dt$. (e and f) Same as (c and d) but the data is sorted by the modified coupling function $d\Phi_{MP}^*/dt$ (Equation 2). The vertical bars denote the standard errors of the means. Note the log scale for the proton flux.

Figures 3a and 3b show that for a fixed value of $d\Phi_{MP}/dt$, the proton flux is clearly greater for $B_y < 0$ than for $B_y > 0$ in both hemispheres, in agreement with the above simulation results. In NH the fluxes are about 30%–50% higher for $B_y < 0$ than for $B_y > 0$ (note the log-scale in Figure 3). The B_y -dependence is even stronger in SH. The proton fluxes are generally higher in SH than NH, probably due to hemispheric asymmetry of magnetic field strength related to the South Atlantic Anomaly. Figures 3c and 3d further quantify the size of the B_y -dependence showing averages of the proton fluxes for $B_y < 0$ and $B_y > 0$ as a function of $d\Phi_{MP}/dt$. The standard errors in Figures 3c and 3d are calculated by normalizing the standard deviation on each bin by the square root of the number of samples. The B_y -effect is present in both hemispheres, although it is stronger for SH. Note that the flux units are shown in logarithmic scale.

Assuming that the fluxes measured by NOAA POES satellites (on low-Earth orbit) reflect patterns in underlying equatorial population, this result strongly supports the above CIMI results on B_y dependence of equatorial ring current fluxes. Figure S2 in Supporting Information S1 repeats the analysis of Figure 3 separately for 0° and 90° telescopes. The B_y -dependencies of both 0° and 90° proton fluxes are very similar, giving further confidence on the robustness of the results.

HOLAPPA AND BUZULUKOVA 5 of 11



Figures S4a and S4b in Supporting Information S1 show the same analysis as Figure 3 for NH winter (dipole tilt $<-20^{\circ}$). These Figures clearly show that the B_y -dependence is reversed in the NH winter, in agreement with earlier studies on the explicit B_y -effect. Figures S4c and S4d in Supporting Information S1 show that the explicit B_y -dependence largely disappears during equinox conditions (absolute value of dipole tilt $<10^{\circ}$). Thus, the flux of energetic protons are enhanced when the dipole tilt and IMF B_y have opposite signs. This suggests that the explicit B_y -dependence can be taken into account in solar wind coupling functions by including an analytical correction factor, which increases (decreases) when the signs of dipole tilt and B_y are opposite (same). Here we propose a modified Newell function

$$d\Phi_{MP}^*/dt = (1 - 0.04 \cdot \tan(\psi)B_{y}) d\Phi_{MP}/dt, \tag{2}$$

where ψ is the dipole tilt angle and the unit of B_y is nT. The correction factor $(1-0.04 \cdot \tan(\psi)B_y)$ fluctuates around one (staying positive for all realistic values of ψ and B_y), and does not affect the long-term averages of the original coupling function. Figures 3e and 3f are similar to Figures 3c and 3d, but use the modified coupling function. Figures 3e and 3f show that sorting the proton fluxes with $d\Phi_{MP}^*/dt$ largely removes the explicit B_y -dependence in the NH for the whole range of $d\Phi_{MP}^*/dt$ used in the analysis. However, the modified function does not completely remove the B_y -dependence in the SH proton fluxes, which indicates a hemispheric asymmetry in the explicit B_y -dependence, especially during strong solar wind driving.

The above SWMF/CIMI model results also suggest that the Dst index exhibits an explicit B_y -dependence. To verify this, we make a similar analysis using the measured Dst, Dst^* index and their rate of change. Figure 4a shows the average measured Dst index as a function of 3-hr means of $d\Phi_{MP}/dt$ and IMF B_y during NH summer (dipole tilt >20°) in the same format as in Figure 3. Figure 4a shows asymmetric pattern with respect to B_y , but the dependence it not so clear as for the proton precipitation. This is likely due the long memory of the Dst index, that is, there is a large lag between solar wind driving (coupling functions) and the response of the Dst index, because the value of Dst index for any give hour is mainly determined by the pre-existing ring current population. However, the time-derivative of the Dst index is known to have a more immediate response (Burton et al., 1975; Newell et al., 2007). Indeed, there is a clear B_y -dependence in ΔDst (Figure 4b), which is the change of the Dst index over 3 hr. The B_y -dependence of Dst and ΔDst are further quantified in Figures 4c and 4d, which show the averages of the Dst index and ΔDst for $B_y < 0$ and $B_y > 0$ during different values of $d\Phi_{MP}/dt$. Analysis of error bars indicates that the effect is stronger for ΔDst and more statistically significant, but it is still present for Dst index as well. Figures 4e and 4f show that the explicit B_y -dependence of Dst and ΔDst are largely accounted for by the modified coupling function $d\Phi_{MP}^*/dt$.

Thus, the ring current grows at a faster rate $(-\Delta Dst)$ is greater) for $B_y < 0$ during positive dipole tilt, confirming the CIMI modeling results on the ring current energy content and model Dst index (Figure 2). Figure S5 in Supporting Information S1 shows the same analysis of Dst and ΔDst for negative $(<-20^{\circ})$ dipole tilt. The B_y -dependence during negative tilt is reversed (faster growth of the ring current for $B_y > 0$) which is also expected from earlier studies on the explicit B_y -effects. The B_y -dependence in the time-derivative of the Dst-index is quite strong. For the highest values of the Newell coupling function shown in Figure 4d ΔDst is about 50% greater for $B_y < 0$ than for $B_y > 0$. In order to have sufficient statistics, data in Figure 4 are limited to mainly non-storm times (as seen in the scale of Dst values in Figure 4a). Further modeling and event studies are needed for studying how significant the B_y -dependence is during storm-times. Figures S6a–S6d in Supporting Information S1 repeat the analysis of Figure 4 for positive and negative dipole tilts using the pressure-corrected Dst index (Dst^*) (O'Brien & McPherron, 2000), yielding practically identical results. This gives confidence that the results of Figure 4 are not contaminated by the magnetopause current.

It should also be noted that IMF B_y is statistically anticorrelated with IMF B_x . To rule out an alternative hypothesis that the above B_y -effects are due to influence of IMF B_x , we repeat the analysis of Figure 4 for two different selections of data. Figure S7 in Supporting Information S1 is similar to Figure 4, but the Dst index is sorted by IMF B_x while requiring that IMF B_y is small ($IB_yI < 2$ nT). Figure S7 in Supporting Information S1 shows that there is no statistically significant B_x -dependence in Dst or ΔDst . These results are consistent with weak <10% B_x -dependence of field-aligned currents found by Laundal et al. (2018). Therefore, we are confident that the explicit B_y -effect studied here is not due to IMF B_x .

HOLAPPA AND BUZULUKOVA 6 of 11



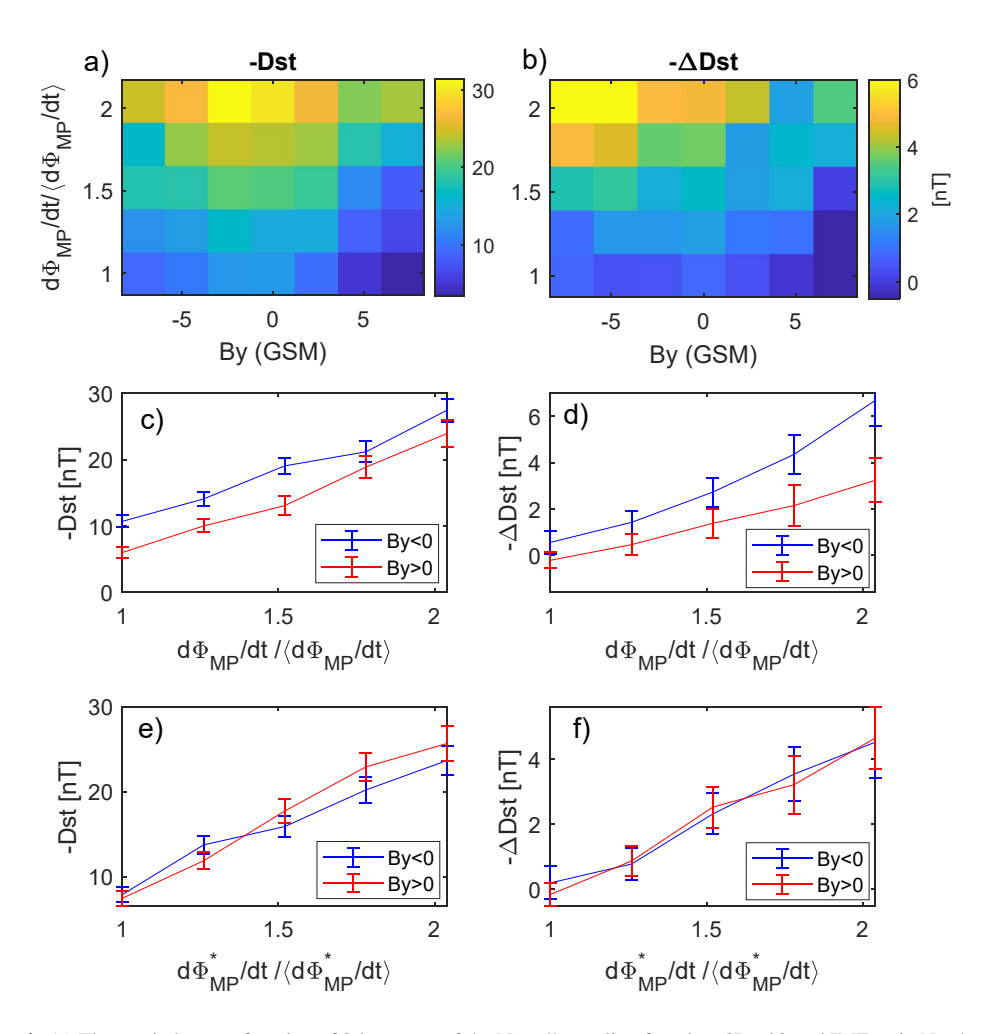


Figure 4. (a) The Dst index as a function of 3-hr means of the Newell coupling function $d\Phi_{MP}/dt$ and IMF B_y in Northern Hemisphere summer (dipole tilt >20°). (b) The change of the Dst index (ΔDst) during the same 3-hr intervals as in the panel (a). Bottom panels show (c) Dst (d) ΔDst averaged for $B_y < 0$ (blue line) and $B_y > 0$ (red line) as a function of Φ_{MP}/dt . (e and f) Same as (c and d), but using the modified coupling function $d\Phi_{MP}^*/dt$. The vertical bars denote the standard errors of the means.

Taken together, the analysis of NOAA POES data and Dst index gives strong evidence that there is a *global* explicit IMF B_y -effect in magnetospheric energetic protons and ring current energy content. These findings are strongly supported by the above SWMF/CIMI results as well.

5. Discussion and Conclusions

It has been known for a long time that IMF B_y plays a role in solar wind-magnetosphere interaction which is seen, for example, convection patterns in polar caps and auroral zones (Cowley et al., 1991; Heppner & Maynard, 1987; Ruohoniemi & Greenwald, 1996, 2005; Thomas & Shepherd, 2018). Recent studies have revealed that IMF B_y effects are complex and seasonally varying, showing dependence on the dipole tilt angle. The combined dependence on IMF B_y and the dipole tilt (also called the explicit B_y -dependence) strongly modulates auroral electrojets (Friis-Christensen et al., 2017; Holappa & Mursula, 2018; Holappa et al., 2021; Workayehu et al., 2021), electron precipitation (Holappa et al., 2020), and the size of polar cap (Reistad et al., 2020). These effects are quite significant, for example, showing variations in the AL index up to 40% for opposite values of B_y .

In this paper, using a global MHD/ring current model and satellite measurements we have demonstrated, for the first time, a global explicit IMF B_v -dependence of the ring current proton fluxes, and the Dst index. We showed

HOLAPPA AND BUZULUKOVA 7 of 11



that IMF B_y -component significantly modulates energetic magnetospheric protons, the time-derivative of the Dst index and consequently the growth-rate of the ring current.

First we performed two simulations with the SWMF coupled with the CIMI inner magnetosphere model with static solar wind/IMF inputs (V = 500 km/s, $B_z = -5 \text{ nT}$) and positive ($+20^\circ$) dipole tilt. The two runs had identical solar wind inputs and other settings except for the sign of IMF B_y . We found that the run with negative B_y produced stronger fluxes of energetic protons in the inner magnetosphere.

To verify the model results we quantified the explicit B_y -dependence of the energetic (30–80 keV) magnetospheric proton fluxes measured by NOAA POES satellites flying on polar low-Earth orbits. We showed that for fixed value of the Newell solar wind coupling function $(d\Phi_{MP}/dt)$ the NOAA POES proton fluxes are greater for $B_y < 0$ than for $B_y > 0$ in NH summer (dipole tilt >20°). These empirical results are in excellent agreement with the model results, assuming that the proton fluxes measured by NOAA POES satellites on low-Earth orbit reflect the modeled equatorial ring current protons with similar energy (IMF B_y not significantly modulating the pitch-angle distribution).

Because the ring current is mainly carried by energetic protons in the inner magnetosphere, the above results indicate that the ring current energy content and the Dst index should also exhibit an explicit IMF B_y dependence. Indeed, we found that the SWMF/CIMI run with a negative IMF B_y produced a greater energy content of the ring current and a more negative modeled Dst index. To verify this empirically, we showed that for a fixed value of $d\Phi_{MP}/dt$ the measured Dst index, Dst^* index and the time-derivatives of Dst and Dst^* (ΔDst , ΔDst^*) is more negative for $B_y < 0$ than for $B_y > 0$ during positive dipole tilt.

Thus, for fixed solar wind driving the ring current grows faster and becomes stronger for $B_y < 0$ ($B_y > 0$) in NH summer (winter). Therefore the ring current growth-rate exhibits a similar explicit B_y -dependence as the westward electrojet (Holappa & Mursula, 2018) and substorm occurrence frequency (Liou et al., 2020; Ohma et al., 2021).

We also showed that the explicit B_y -dependence of energetic proton fluxes in the NH, Dst and ΔDst can be accounted for using a modified solar wind coupling function $d\Phi_{MP}^*/dt = (1-0.04\tan(\psi)By) \cdot d\Phi_{MP}/dt$ (see Equation 2), where the correction factor $(1-0.04\tan(\psi)By)$ is greater/smaller than 1 for opposite/same signs of the dipole tilt ψ and B_y . We also found that the modified function does not work as well for the SH proton fluxes, indicating a hemispheric asymmetry in the B_y -dependence. It is surprising though that the same modification works well eliminating the asymmetry both for ΔDst and proton fluxes, at least for the NH. Further studies are needed for better quantification of the hemispheric differences and their physical causes.

The physical mechanism(s) of the explicit B_y -effects on the magnetospheric dynamics and particularly on the inner magnetosphere are still not fully understood. Recently, Reistad et al. (2020) used the equatorward boundary of the region 1 current system as a proxy for the polar cap size and showed that the polar cap area exhibits a similar explicit B_y -dependence: during positive tilt polar cap is larger for $B_y < 0$ than for $B_y > 0$ while the B_y -dependence is opposite for negative dipole tilt. They suggested that IMF B_y either modulates the dayside reconnection rate or the magnetotail response to solar wind driving. Evidence toward the former hypothesis was provided by Reistad et al. (2021) who showed that there is an explicit B_y -dependence in the cross-polar cap potential which is consistent with a similar B_y -dependence of the substorm occurrence frequency (Liou et al., 2020; Ohma et al., 2021).

The IMF B_y -dependence of the energetic proton fluxes and the ring current in the inner magnetosphere is probably closely related to the B_y -dependence of substorm activity, as substorms are known to cause injections of energetic particles into the inner magnetosphere (Birn et al., 1998; Gkioulidou et al., 2014; Mauk & McIlwain, 1974). Another explanation is suggested by results from ring current models showing that electric field in the inner magnetosphere controls the strength of the ring current (e.g., Ebihara & Ejiri, 2003). In order to get stronger ring current in the coupled model, there should be a stronger potential drop and stronger convection near the ring current model polar boundary, that is, on closed magnetic field lines. From this perspective it would be interesting to reanalyze the results of C:son Brandt et al. (2002) to examine if strong IMF B_y produces additional skewing of the electric field in the inner magnetosphere. Multiple studies confirm that the presence of IMF B_y is not needed for the skewing since it is produced by the ring current itself (Buzulukova, Fok, Goldstein, et al., 2010; Ebihara & Fok, 2004; M. C. Fok et al., 2003; Wolf, 1983). However, the results of our study suggest that indeed some additional effect is possible since the strength of the ring current is modulated by IMF B_y . At present, it is not clear why the convection on the closed field lines should be stronger when the signs of IMF B_y and dipole tilt are

HOLAPPA AND BUZULUKOVA 8 of 11



opposite. However the reproduction of the effect with the coupled SWMF/CIMI model demonstrates the potential of future modeling studies to uncover the physical mechanism of the explicit B_y -effect. Further modeling and event-based studies are also needed for studying how significant the explicit B_y -dependence of the ring current is during storm-times.

Data Availability Statement

Detailed model settings (PARAM.in files) and model output used in production of Figures 1 and 2 have been made available online for download at Zenodo (https://doi.org/10.5281/zenodo.6459937). SWMF run input files are also included in Text S8 and S9 of Supporting Information S1. The solar wind data (solar wind speed and different components of IMF) and the *Dst* index were downloaded from the OMNI2 database (http://omniweb.gsfc.nasa.gov/). All the original POES/MEPED energetic particle data used here are archived in the NOAA/ NGDC dataserver (http://www.ngdc.noaa.gov/stp/satellite/poes/index.html).

Acknowledgments References

The authors acknowledge the financial

to the Postdoctoral Researcher project

support by the Academy of Finland

of L. Holappa (no. 322459). For N.

Y. Buzulukova, this work has been

partially supported by NASA Grant

80NSSC19K0085. N. Y. Buzulukova

thanks ISSI in Bern Switzerland for

support of the International Team N523

Magnetosphere." This work was carried

out using the SWMF and BATS-R-US

tools developed at the University of

Michigan Center for Space Environ-

ment Modeling. The modeling tools are

part of the Full version of SWMF code

that is available for download under a

user license through the University of

Michigan web-page http://csem.engin.

umich.edu/swmf. CIMI model has been

division, Geospace Physics Laboratory.

Computational resources supporting

this work were provided by the NASA

High-End Computing Program through

the NASA Advanced Supercomputing

Division at Ames Research Center.

developed at NASA GSFC, Heliophysics

"Imaging the Invisible: Unveiling the

Global Structure of Earth's Dynamic

- Asikainen, T., & Mursula, K. (2011). Recalibration of the long-term NOAA/MEPED energetic proton measurements. *Journal of Atmospheric and Solar-Terrestrial Physics*, 73(2–3), 335–347. https://doi.org/10.1016/j.jastp.2009.12.011
- Asikainen, T., & Mursula, K. (2013). Correcting the NOAA/MEPED energetic electron fluxes for detector efficiency and proton contamination. Journal of Geophysical Research, 118(10), 6500–6510. https://doi.org/10.1002/jgra.50584
- Birn, J., & Hesse, M. (2013). The substorm current wedge in MHD simulations. *Journal of Geophysical Research: Space Physics*, 118(6), 3364–3376. https://doi.org/10.1002/jgra.50187
- Birn, J., Thomsen, M. F., Borovsky, J. E., Reeves, G. D., McComas, D. J., Belian, R. D., & Hesse, M. (1998). Substorm electron injections: Geosynchronous observations and test particle simulations. *Journal of Geophysical Research*, 103(A5), 9235–9248. https://doi.org/10.1029/97JA02635
- Burton, R. K., McPherron, R. L., & Russell, C. T. (1975). An empirical relationship between interplanetary conditions and Dst. *Journal of Geophysical Research*, 80(31), 4204–4214. https://doi.org/10.1029/ja080i031p04204
- Buzulukova, N., Fok, M.-C., Goldstein, J., Valek, P., McComas, D. J., & C:son Brandt, P. C. (2010). Ring current dynamics in moderate and strong storms: Comparative analysis of TWINS and IMAGE/HENA data with the Comprehensive Ring Current Model. *Journal of Geophysical Research*, 115(A12). https://doi.org/10.1029/2010JA015292
- Buzulukova, N., Fok, M.-C., Pulkkinen, A., Kuznetsova, M., Moore, T. E., Glocer, A., et al. (2010). Dynamics of ring current and electric fields in the inner magnetosphere during disturbed periods: CRCM–BATS-R-US coupled model. *Journal of Geophysical Research*, 115(A5). https://doi.org/10.1029/2009ja014621
- Cowley, S. W. H., Morelli, J. P., & Lockwood, M. (1991). Dependence of convective flows and particle precipitation in the high-latitude dayside ionosphere on the x and y components of the interplanetary magnetic field. *Journal of Geophysical Research*, 96(A4), 5557–5564. https://doi. org/10.1029/90ja02063
- C:son Brandt, P., Ohtani, S., Mitchell, D. G., Fok, M.-C., Roelof, E. C., & Demajistre, R. (2002). Global ENA observations of the storm mainphase ring current: Implications for skewed electric fields in the inner magnetosphere. *Geophysical Research Letters*, 29(20). 15-1–15-3. https://doi.org/10.1029/2002GL015160
- Dessler, A. J., & Parker, E. N. (1959). Hydromagnetic theory of geomagnetic storms. *Journal of Geophysical Research*, 64(12), 2239–2252. https://doi.org/10.1029/jz064i012p02239
- de Zeeuw, D. L., Sazykin, S., Wolf, R. A., Gombosi, T. I., Ridley, A. J., & Tóth, G. (2004). Coupling of a global MHD code and an inner magnetospheric model: Initial results. *Journal of Geophysical Research*, 109(A12), A12219. https://doi.org/10.1029/2003JA010366
- Dungey, J. W. (1961). Interplanetary magnetic field and the auroral zones. *Physical Review Letters*, 6(2), 47–49. https://doi.org/10.1103/physrevlett.6.47
- Ebihara, Y., & Ejiri, M. (2003). Numerical simulation of the ring current: Review. Space Science Reviews, 105(1), 377–452. https://doi.org/10.1023/A:1023905607888
- $Ebihara, Y., \& Fok, M. C. (2004). Postmidnight storm-time enhancement of tens-of-keV proton flux. \textit{Journal of Geophysical Research}, 109 (A12), \\ A12209. \ https://doi.org/10.1029/2004JA010523$
- Fedder, J. A., Slinker, S. P., Lyon, J. G., & Elphinstone, R. D. (1995). Global numerical simulation of the growth phase and the expansion onset for a substorm observed by Viking. *Journal of Geophysical Research*, 100(A10), 19083–19093. https://doi.org/10.1029/95JA01524
- Fok, M.-C., Buzulukova, N. Y., Chen, S.-H., Glocer, A., Nagai, T., Valek, P., & Perez, J. D. (2014). The comprehensive inner magnetosphere-ion-osphere model. *Journal of Geophysical Research: Space Physics*, 119(9), 7522–7540. https://doi.org/10.1002/2014ja020239
- Fok, M.-C., Kang, S.-B., Ferradas, C. P., Buzulukova, N. Y., Glocer, A., & Komar, C. M. (2021). New developments in the comprehensive inner magnetosphere-ionosphere model. *Journal of Geophysical Research: Space Physics*, 126(4), e2020JA028987. https://doi.org/10.1029/2020ja028987
- Fok, M. C., Moore, T. E., Wilson, G. R., Perez, J. D., Zhang, X. X., C:Son Brandt, P. C., et al. (2003). Global ENA image simulations. *Space Science Reviews*, 109(1), 77–103. https://doi.org/10.1023/B:SPAC.0000007514.56380.fd
- Friis-Christensen, E., Finlay, C. C., Hesse, M., & Laundal, K. M. (2017). Magnetic field perturbations from currents in the dark polar regions during quiet geomagnetic conditions. Space Science Reviews, 206(1-4), 281-297. https://doi.org/10.1007/s11214-017-0332-1
- Friis-Christensen, E., Lassen, K., Wilhjelm, J., Wilcox, J. M., Gonzalez, W., & Colburn, D. S. (1972). Critical component of the interplanetary magnetic field responsible for large geomagnetic effects in the polar cap. *Journal of Geophysical Research*, 77(19), 3371–3376. https://doi.org/10.1029/JA077i019p03371
- Gkioulidou, M., Ukhorskiy, A. Y., Mitchell, D. G., Sotirelis, T., Mauk, B. H., & Lanzerotti, L. J. (2014). The role of small-scale ion injections in the buildup of Earth's ring current pressure: Van Allen Probes observations of the 17 March 2013 storm. *Journal of Geophysical Research: Space Physics*, 119(9), 7327–7342. https://doi.org/10.1002/2014ja020096

HOLAPPA AND BUZULUKOVA 9 of 11



- Glocer, A., Fok, M., Meng, X., Toth, G., Buzulukova, N., Chen, S., & Lin, K. (2013). CRCM+ BATS-R-US two-way coupling. *Journal of Geophysical Research: Space Physics*, 118(4), 1635–1650. https://doi.org/10.1002/jgra.50221
- Gordeev, E., Sergeev, V., Tsyganenko, N., Kuznetsova, M., Rastter, L., Raeder, J., et al. (2017). The substorm cycle as reproduced by global MHD models. Space Weather, 15(1), 131–149. https://doi.org/10.1002/2016SW001495
- Hamilton, D. C., Gloeckler, G., Ipavich, F., Stüdemann, W., Wilken, B., & Kremser, G. (1988). Ring current development during the great geomagnetic storm of February 1986. Journal of Geophysical Research, 93(A12), 14343–14355. https://doi.org/10.1029/ja093ia12p14343
- Heppner, J. P., & Maynard, N. C. (1987). Empirical high-latitude electric field models. *Journal of Geophysical Research*, 92(A5), 4467–4489. https://doi.org/10.1029/ja092ia05p04467
- Holappa, L., Asikainen, T., & Mursula, K. (2020). Explicit IMF dependence in geomagnetic activity: Modulation of precipitating electrons. Geophysical Research Letters, 47(4), e2019GL086676. https://doi.org/10.1029/2019g1086676
- Holappa, L., & Mursula, K. (2018). Explicit IMF B_y-dependence in high-latitude geomagnetic activity. *Journal of Geophysical Research*, 123(6), 4728–4740. https://doi.org/10.1029/2018JA025517
- Holappa, L., Robinson, R. M., Pulkkinen, A., Asikainen, T., & Mursula, K. (2021). Explicit IMF by-dependence in geomagnetic activity: Quantifying ionospheric electrodynamics. *Journal of Geophysical Research: Space Physics*, 126(4), e2021JA029202. https://doi.org/10.1029/2021JA029202
- Kan, J. R., & Lee, L. C. (1979). Energy coupling function and solar wind-magnetosphere dynamo. Geophysical Research Letters, 6(7), 577–580. https://doi.org/10.1029/GL006i007p00577
- Keesee, A. M., Buzulukova, N., Mouikis, C., & Scime, E. E. (2021). Mesoscale structures in Earth's magnetotail observed using energetic neutral atom imaging. Geophysical Research Letters, 48(3), e2020GL091467. https://doi.org/10.1029/2020GL091467
- Laitinen, T. V., Palmroth, M., Pulkkinen, T. I., Janhunen, P., & Koskinen, H. E. J. (2007). Continuous reconnection line and pressure-dependent energy conversion on the magnetopause in a global MHD model. *Journal of Geophysical Research*, 112(A11). https://doi.org/10.1029/2007ja012352
- Laundal, K. M., Reistad, J. P., Finlay, C. C., Stgaard, N., Tenfjord, P., Snekvik, K., & Ohma, A. (2018). Interplanetary magnetic field B_x component influence on horizontal and field-aligned currents in the ionosphere. *Journal of Geophysical Research*, 123(5), 3360–3379. https://doi.org/10.1002/2017ja024864
- Liemohn, M. W., Kozyra, J. U., Thomsen, M. F., Roeder, J. L., Lu, G., Borovsky, J. E., & Cayton, T. E. (2001). Dominant role of the asymmetric ring current in producing the stormtime Dst. *Journal of Geophysical Research*, 106(A6), 10883–10904. https://doi.org/10.1029/2000ja000326 Liou, K., & Mitchell, E. (2019). Effects of the interplanetary magnetic field y component on the dayside aurora. *Geoscience Letters*, 6(1), 1–10. https://doi.org/10.1186/s40562-019-0141-3
- Liou, K., & Mitchell, E. J. (2019). Hemispheric asymmetry of the premidnight aurora associated with the dawn-dusk component of the interplanetary magnetic field. *Journal of Geophysical Research: Space Physics*, 124(3), 1625–1634. https://doi.org/10.1029/2018ja025953
- Liou, K., Newell, P. T., Meng, C. I., Brittnacher, M., & Parks, G. (1998). Characteristics of the solar wind controlled auroral emissions. *Journal of Geophysical Research*, 103(A8), 17543–17557. https://doi.org/10.1029/98ja01388
- Liou, K., Sotirelis, T., & Mitchell, E. (2020). Control of the east-west component of the interplanetary magnetic field on the occurrence of magnetic substorms. Geophysical Research Letters, 47(5), e2020GL087406. https://doi.org/10.1029/2020gl087406
- Mauk, B. H., & McIlwain, C. E. (1974). Correlation of K_p with the substorm-injected plasma boundary. *Journal of Geophysical Research*, 79(22), 3193–3196. https://doi.org/10.1029/JA079i022p03193
- Merkin, V. G., Panov, E. V., Sorathia, K. A., & Ukhorskiy, A. Y. (2019). Contribution of bursty bulk flows to the global dipolarization of the magnetotail during an isolated substorm. *Journal of Geophysical Research: Space Physics*, 124(11), 8647–8668. https://doi.org/10.1029/2019JA026872
- Murayama, T., Aoki, T., Nakai, H., & Hakamada, K. (1980). Empirical formula to relate the auroral electrojet intensity with interplanetary parameters. *Planetary and Space Science*, 28(8), 803–813. https://doi.org/10.1016/0032-0633(80)90078-1
- Newell, P. T., Sotirelis, T., Liou, K., Meng, C.-I., & Rich, F. J. (2007). A nearly universal solar wind-magnetosphere coupling function inferred from 10 magnetospheric state variables. *Journal of Geophysical Research*, 112(A1). https://doi.org/10.1029/2006ja012015
- O'Brien, T. P., & McPherron, R. L. (2000). An empirical phase space analysis of ring current dynamics: Solar wind control of injection and decay. Journal of Geophysical Research, 105(A4), 7707–7719. https://doi.org/10.1029/1998ja000437
- Ohma, A., Reistad, J. P., & Hatch, S. M. (2021). Modulation of magnetospheric substorm frequency: Dipole tilt and IMF by effects. *Journal of Geophysical Research: Space Physics*, 126(3), e2020JA028856.
- Perreault, P., & Akasofu, S.-I. (1978). A study of geomagnetic storms. Geophysical Journal of the Royal Astronomical Society, 54(3), 547–573. https://doi.org/10.1111/j.1365-246x.1978.tb05494.x
- Powell, K. G., Roe, P. L., Linde, T. J., Gombosi, T. I., & De Zeeuw, D. L. (1999). A solution-adaptive upwind scheme for ideal magnetohydrodynamics. *Journal of Computational Physics*, 154(2), 284–309. https://doi.org/10.1006/jcph.1999.6299
- Raeder, J., Zhu, P., Ge, Y., & Siscoe, G. (2010). Open geospace general circulation model simulation of a substorm: Axial tail instability and ballooning mode preceding substorm onset. *Journal of Geophysical Research*, 115(A5). https://doi.org/10.1029/2010JA015876
- Reistad, J. P., Laundal, K. M., Ohma, A., Moretto, T., & Milan, S. E. (2020). An explicit IMF by dependence on solar wind-magnetosphere
- coupling. Geophysical Research Letters, 47(1), e2019GL086062.
 Reistad, J. P., Laundal, K. M., Østgaard, N., Ohma, A., Burrell, A. G., Hatch, S. M., et al. (2021). Quantifying the lobe reconnection rate during
- dominant IMF B_y periods and different dipole tilt orientations. *Journal of Geophysical Research: Space Physics*, 126(11), e2021JA029742. Ridley, A. J., Gombosi, T. I., & De Zeeuw, D. L. (2004). Ionospheric control of the magnetosphere: Conductance. *Annales Geophysicae*, 22(2),
- 567–584. https://doi.org/10.5194/angeo-22-567-2004
 Rodger, C. J., Carson, B. R., Cummer, S. A., Gamble, R. J., Clilverd, M. A., Green, J. C., et al. (2010). Contrasting the efficiency of radiation belt losses caused by ducted and nonducted whistler-mode waves from ground-based transmitters. *Journal of Geophysical Research*, 115(A12).
- https://doi.org/10.1029/2010ja015880

 Ruohoniemi, J. M., & Greenwald, R. A. (1996). Statistical patterns of high-latitude convection obtained from Goose Bay HF radar observations.
- Journal of Geophysical Research, 101(A10), 21743–21763. https://doi.org/10.1029/96JA01584
 Ruohoniemi, J. M., & Greenwald, R. A. (2005). Dependencies of high-latitude plasma convection: Consideration of interplanetary magnetic field,
- seasonal, and universal time factors in statistical patterns. *Journal of Geophysical Research*, 110(A9). https://doi.org/10.1029/2004ja010815 Shue, J.-H., Newell, P., Liou, K., & Meng, C.-I. (2001). Influence of interplanetary magnetic field on global auroral patterns. *Journal of Geophysical Research*, 106(A4), 5913–5926. https://doi.org/10.1029/2000ja003010
- Smith, A. R. A., Beggan, C. D., Macmillan, S., & Whaler, K. A. (2017). Climatology of the auroral electrojets derived from the along-track gradient of magnetic field intensity measured by POGO, Magsat, CHAMP, and Swarm. Space Weather, 15(10), 1257–1269. https://doi.org/10.1002/2017SW001675

HOLAPPA AND BUZULUKOVA 10 of 11





- Sonnerup, B. U. O. (1974). Magnetopause reconnection rate. Journal of Geophysical Research, 79(10), 1546–1549. https://doi.org/10.1029/ JA079i010p01546
- Thomas, E. G., & Shepherd, S. G. (2018). Statistical patterns of ionospheric convection derived from mid-latitude, high-latitude, and polar Super-DARN HF radar observations. *Journal of Geophysical Research*, 123(4), 3196–3216. https://doi.org/10.1002/2018ja025280
- Tóth, G., Sokolov, I. V., Gombosi, T. I., Chesney, D. R., Clauer, C. R., De Zeeuw, D. L., et al. (2005). Space Weather Modeling Framework: A new tool for the space science community. *Journal of Geophysical Research*, 110(A12), A12226. https://doi.org/10.1029/2005ja011126
- Tóth, G., Van der Holst, B., Sokolov, I. V., De Zeeuw, D. L., Gombosi, T. I., Fang, F., et al. (2012). Adaptive numerical algorithms in space weather modeling. *Journal of Computational Physics*, 231(3), 870–903. https://doi.org/10.1016/j.jcp.2011.02.006
- Trattner, K. J., Petrinec, S. M., Fuselier, S. A., & Phan, T. D. (2012). The location of reconnection at the magnetopause: Testing the maximum magnetic shear model with THEMIS observations. *Journal of Geophysical Research*, 117(A1). https://doi.org/10.1029/2011ja016959
- Velichko, V. A., Boroyev, R. N., Gelberg, M. G., Baishev, D. G., Olson, J. V., Morris, R. J., & Yumoto, K. (2002). North-south asymmetry of the substorm intensity depending on the IMF B_Y-component. *Earth Planets and Space*, 54(10), 955–961. https://doi.org/10.1186/bf03352443
- Weimer, D., & Edwards, T. (2021). Testing the electrodynamic method to derive height-integrated ionospheric conductances. *Annales Geophysicae*, 39(1), 31–51. https://doi.org/10.5194/angeo-39-31-2021
- Wolf, R. A. (1983). The quasi-static (slow-flow) region of the magnetosphere. In R. L.Carovillano & J. M. Forbes (Eds.), Solar-terrestrial physics: Principles and theoretical foundations. Astrophysics and Space Science Library (Vol. 104, pp. 303–368). https://doi.org/10.1007/978-94-009-7194-3_14
- Workayehu, A. B., Vanhamäki, H., Aikio, A. T., & Shepherd, S. G. (2021). Effect of interplanetary magnetic field on hemispheric asymmetry in ionospheric horizontal and field-aligned currents during different seasons. *Journal of Geophysical Research: Space Physics*, 126(10), e2021JA029475. https://doi.org/10.1029/2021ja029475
- Yakovchouk, O. S., Mursula, K., Holappa, L., Veselovsky, I. S., & Karinen, A. (2012). Average properties of geomagnetic storms in 1932–2009. Journal of Geophysical Research, 117(A3), A03201. https://doi.org/10.1029/2011JA017093
- Zhang, J., Liemohn, M. W., De Zeeuw, D. L., Borovsky, J. E., Ridley, A. J., Toth, G., et al. (2007). Understanding storm-time ring current development through data-model comparisons of a moderate storm. *Journal of Geophysical Research*, 112(A4). https://doi.org/10.1029/2006ja011846

HOLAPPA AND BUZULUKOVA 11 of 11